Acoustic pulse propagation and localization in bubbly water

Kang-xin Wang and Zhen Ye
Wave Phenomena Laboratory, Department of Physics, National Central University, Chungli, Taiwan 32054, Republic of China
(Received 8 May 2001; published 22 October 2001)

Acoustic pulse propagation in bubbly water is studied using a self-consistent method. The acoustic transmission and backscattering are evaluated numerically. Under proper conditions, the localization of acoustic waves is identified within a range of frequency. The results show that when a short pulse is transmitted the waves of frequencies within the localization regime will be trapped in the system and reveal a coherent behavior. A phase diagram approach is used to describe the localization behavior.

DOI: 10.1103/PhysRevE.64.056607 PACS number(s): 43.20.+g

I. INTRODUCTION

The propagation of waves through random media continues to be the subject of vivid research [1–5]. By analogy with the well-known localization of the electron transport in disordered condensed matters arising from the interference effects in multiple scattering [6,7], it has been discussed much in the literature that similar localization may also exist in the transmission of the classical waves in random media when the multiple scattering becomes strong [8–16]. Such a localization phenomenon has been characterized by two levels. One is the weak localization associated with the enhanced backscattering. The second is termed as the strong localization in which a significant inhibition of transmission surfaces indicating that the energy is mostly confined in a region of space in the neighborhood of the emission. In other words, under certain conditions, the wave can be trapped in a spatial domain.

Considerable efforts have been devoted to propagation of classical waves in random media. While the weak localization, regarded as a precursor to the strong localization, has been well studied theoretically and observed experimentally [17], the phenomenon of strong localization in three dimensions has also been reported in a number of systems. Random underwater topography can give rise to water wave localization [18]. Localization effects have also been reported for microwaves [13], for light [19], and for acoustic waves [20] in disordered media.

In a recent paper [21], we have shown that localization may be achieved for acoustic waves propagation in water with even a very small fraction of air-filled spherical bubbles, supporting in part the previous conjecture [10]. It is shown that the localization appears within a region of frequency slightly above the natural frequency of the individual air bubbles. Outside this region, wave propagation remains extended. In this paper, we present a further numerical investigation of acoustic localization in bubbly water. In particular, we consider the propagation of acoustic pulses through water having many air-filled bubbles. Such a random medium can be either generated in experimental laboratories or can be commonly found at ocean surfaces where the bubbles are generated by breaking waves. Unlike most previous approaches that derive approximately a diffusion equation for the ensemble averaged energy, our method is to solve the scattering problem from the fundamental wave equations. The approach is based on a genuine self-consistent scheme following the procedure of Twersky [4] reviewed in Ref. [22], and has been discussed in Ref. [23]. In the approach, the wave propagation is represented by a set of coupled equations and is solved rigorously. Wave transmission and backscattering are thus obtained. We investigate how the acoustic waves are established in the medium after the pulses are transmitted. A different method is proposed to describe the phase transition between localized and extended states. The approach enables to isolate the localization effect from the residual absorption effect; the inability to discriminate the localization effect from the absorption effect has caused considerable debate in the literature with regard to the claimed observation of wave localization being actually due to the absorption [24].

Before moving on, we point out that considerable efforts from both theoretical and experimental point of view have been devoted to propagation of acoustic waves in bubbly liquids. A review on general aspects of the subject may be found in the monography [25]. The strong localization of acoustic waves in bubbly liquids was first suggested by Sornette and Souillard [10]. But no detailed results were given. Later, acoustic wave propagation in bubbly waters was also studied using the perturbative diagrammatic method [26,27]. Including a higher order correction representing the mutual interaction between two bubbles, their results show that when the concentration of the bubbles reaches a certain value, the wave phase speed can become negative; one of their suggestions is the appearance of wave trapping. An obvious shortcoming of the diagrammatic approach, however, is that it cannot exclude the possibility of the breakdown of the perturbative calculation, and how many and what type of perturbation terms should be included are unknown. In order to gain a definite insight into the problem, it is therefore highly desirable that one can study the problem in a rigorous or an effectively exact manner. Although this is virtually impossible for systems containing an infinite number of scatterers, the rigorous results can be obtained for systems consisting of a finite number of scatterers. This paper is one of such studies.

The paper is organized as follows. The general theory is presented in the following section, followed by some approximations. The theoretical model and the results are presented in Sec. III. A summary concludes this paper in Sec. IV.

 ©2001 The American Physical Society

II. THEORY

A. Pulses generation

We consider a point acoustic source in a medium. The source is located at $\vec{r}_0$, and is transmitting acoustic pulses in all directions. The wave equation for the acoustic wave propagation in the medium can then be written as

$$\left(\nabla^2-\frac{1}{c^2(\vec{r})}\frac{\partial^2}{\partial t^2}\right)p(\vec{r},t)=-4\pi\delta^{(3)}(\vec{r}-\vec{r}_0)s(t), \quad (1)$$

where $c(\vec{r})$ is the sound speed in the medium, and the time-dependent source term $s(t)$ reflects the temporal aspect of the acoustic source. Inside the scatterer the sound speed is c_1 while that of the surrounding medium is c. In the following, we assume that the source is located at the origin, i.e., $r_0=0$.

Upon the Fourier transformation, Eq. (1) becomes

$$\left(\nabla^2+\frac{\omega^2}{c^2(\vec{r})}\right)p(\vec{r},\omega)=-4\pi\delta^{(3)}(\vec{r})S(\omega), \quad (2)$$

where we used

$$p(\vec{r},t)=\frac{1}{2\pi}\int_{-\infty}^{\infty}d\omega\, e^{-i\omega t}p(\vec{r},\omega), \quad (3)$$

and

$$s(t)=\frac{1}{2\pi}\int_{-\infty}^{\infty}d\omega\, e^{-i\omega t}S(\omega). \quad (4)$$

We have considered two types of pulse shapes. (a) For broad band pulses, we have

$$s(t)=\begin{cases}0, & t<0\\ e^{-\alpha t}, & t\geqslant 0.\end{cases} \quad (5)$$

This gives

$$S(\omega)=\frac{1}{2(\alpha-i\omega)}. \quad (6)$$

For small ω $(\omega\ll\alpha)$, the spectral density is approximately a constant: $s(\omega)\approx 2\pi/\alpha$. (b) The narrow band pulses are also considered. In this case,

$$s(t)=\begin{cases}\cos\omega_0 t, & -b<t<b \ \text{ and } \ \omega_0 b\gg 1\\ 0, & |t|>b.\end{cases} \quad (7)$$

Then the spectral density is found as

$$S(\omega)=\frac{\sin(\omega+\omega_0)b}{2\pi(\omega+\omega_0)}+\frac{\sin(\omega-\omega_0)}{2\pi(\omega-\omega_0)}. \quad (8)$$

The Gaussian pulses may also be considered. We found that the results are qualitatively the same for different pulse shapes. For simplicity, we only present the results for the broad band pulses.

B. Scattering by an ensemble of scattering spheres

Although in the later part of the paper we will focus on the low frequency acoustic scattering by air bubbles for which a much simplified scheme can be developed, for completeness and future uses, here we would like to present a general scattering theory for many scatterers that is valid for all frequencies and any configuration of bubble clouds. Consider a wave being scattered by N spherical scatterers, located at $\vec{r}_i$ $(i=1,2,\ldots,N.)$ When a wave encounters a target, it will be scattered; and the scattered wave will be scattered consequently by other scatterers, forming a multiple scattering process. After all scattering, the wave will reach a receiver. The multiple scattering in such a scattering system can be conveniently studied by the self-consistent scheme outlined by Twersky [4]. Here we present a brief account of the procedure.

Equation (4) shows that we can first compute the scattering problem for each frequency and the final signal received can be inverted from the inverse Fourier transformation

$$p(\vec{r},t)=\frac{1}{2\pi}\int_{-\infty}^{\infty}d\omega\, e^{-i\omega t}p(\vec{r},\omega). \quad (9)$$

In this section, we will derive a formula for $p(\vec{r},\omega)$.

We take the following convention: For each scatterer, we can associate it with a coordinate system, and use $[\vec{r}]_i$ to denote the coordinates measured from the ith scatterer and use $\vec{r}$ for the coordinates for the global system.

Assume that the scattering wave from the jth scatterer is written as

$$p_s(\vec{r}_j,\vec{r},\omega)=\sum_{l=0}^{\infty}\sum_{m=-l}^{m=l}C_{lm}^{j}h_l^{(1)}(k|\vec{r}-\vec{r}_j|)Y_l^m([\theta,\phi]_j), \quad (10)$$

where $Y_l^m(\theta,\phi)$ is the spherical harmonic, and θ_j and ϕ_j are the two spherical angles measured at the jth scatterer. Hereafter, $k=\omega/c$.

The incident wave on the ith scatterer is equal to the summation of the direct wave from the source and the scattering wave from all other scatterers

$$p_{in}(\vec{r},\omega)=p_0(\vec{r},\omega)+\sum_{j=1,j\neq i}^{\infty}p_s(\vec{r}_j,\vec{r},\omega), \quad (11)$$

where p_0 is the direct wave from the source and equals $S(\omega)e^{ikr}/r$. Here $\vec{r}$ is around the ith scatterer. The incident wave in Eq. (11) can be expanded in terms of the spherical harmonic functions from $\vec{r}_i$,

$$p_{in}([\vec{r}]_i,\omega)=\sum_{l=0}^{\infty}\sum_{m=-l}^{m=l}D_{lm}^{i}j_l(k|\vec{r}-\vec{r}_i|)Y_l^m([\theta,\phi]_i), \quad (12)$$

where j_l is the jth order Bessel function of the first kind; taking j_l prevents the wave from divergence at $\vec{r}=\vec{r}_i$.

By the addition theorem [28], taking the following expansion of the jth scatterer in terms of the ith scatterer

$$h_l^{(1)}(k|\vec{r}-\vec{r}_j|)Y_l^m([\theta,\phi]_j) = \sum_{\alpha=0}^{\infty}\sum_{\beta=-\alpha}^{\beta=\alpha} T_{\alpha\beta}^{lm,ji} j_\alpha(k|\vec{r}-\vec{r}_i|)Y_\alpha^\beta([\theta,\phi]_i), \tag{13}$$

into Eq. (10), we get

$$D_{lm}^i = S_{lm}^i + \sum_{j=1,j\neq i}^{N}\sum_{p=1}^{\infty}\sum_{q=-p}^{q=p} C_{pq}^j T_{lm}^{pq,ji} = S_{lm}^i + \sum_{j=1}^{N}\sum_{p=1}^{\infty}\sum_{q=-p}^{q=p}(1-\delta_{ij})C_{pq}^j T_{lm}^{pq,ji}, \tag{14}$$

where S_{lm}^i is due to the direct incident wave on the ith scatterer and assumed to be known, i.e.,

$$p_0^i(\vec{r},\omega) = \sum_{l=0}^{\infty}\sum_{m=-l}^{m=l} S_{lm}^i j_l(k|\vec{r}-\vec{r}_i|)Y_l^m([\theta,\phi]_i). \tag{15}$$

In Eq. (13), the coefficient $T_{\alpha\beta}^{lm,ji}$ can be solved as

$$T_{\alpha\beta}^{lm,ji} = \int [d\Omega]_i \frac{[h_l^{(1)}(k|\vec{r}-\vec{r}_j|)]_{S_i}}{j_l(ka)} Y_l^m([\theta,\phi]_j)Y_\alpha^\beta([\theta,\phi]_i), \tag{16}$$

where $[h_l^{(1)}(k|\vec{r}-\vec{r}_j|)]_{S_i}$ means taking the value when $\vec{r}$ is located on the surface of the ith scatterer. Please note that $[\theta,\phi]_j$ and $\vec{r}$ also depend on the position of the point on the surface of the ith scatterer.

Now we solve the boundary conditions at the ith scatterer. The wave inside the ith bubble is written as

$$p_{inside}^i = \sum_{l=0}^{\infty}\sum_{m=-l}^{m=l} A_{lm}^i j_l(k_1|\vec{r}-\vec{r}_i|)Y_l^m([\theta,\phi]_i). \tag{17}$$

The boundary conditions state that the pressure and the normal velocity be continuous across the interface between a scatterer and the surrounding medium. From these conditions we have

$$C_{lm}^i h_l^{(1)}(ka) + D_{lm}^i j_l(ka) = A_{lm}^i j_l(k_1 a), \tag{18}$$

and

$$C_{lm}^i h_l^{(1)\prime}(ka) + D_{lm}^i j_l{}'(ka) = \frac{1}{gh} A_{lm}^i j_l'(k_1 a), \tag{19}$$

where $f'(x)=df(x)/dx$, $k_1=\omega/c$, $g=\rho_1/\rho$, and $h=c_1/c$ with c and c_1, ρ and ρ_1 being the sound speeds and mass densities inside the air bubble and in the water medium, respectively.

From Eqs. (18) and (19), we obtain

$$C_{lm}^i \equiv -\Gamma_l D_{lm}^i = -\frac{[j_l(ka)j_l'(k_1a) - ghj_l(k_1a)j_l'(ka)]}{[h_l^{(1)\prime}(ka)j_l'(k_1a) - ghj_l(k_1a)h_l^{(1)\prime}(ka)]} D_{lm}^i. \tag{20}$$

With Eq. (20), the coefficients C_{lm}^i can be obtained from the self-consistent equation (14). Once C_{lm}^i are known, the field at any spatial point can be obtained from

$$p(\vec{r},\omega) = p_0(\vec{r},\omega) + \sum_{j=1}^{N}\sum_{l=0}^{\infty}\sum_{m=-l}^{m=l} C_{lm}^j h_l^{(1)} \times (k|\vec{r}-\vec{r}_j|)Y_l^m([\theta,\phi]_j). \tag{21}$$

We also note that the present approach also works for elastic spherical scatterers as long as the transfer coefficient $-\Gamma_l$ is modified to take into account the shear modulus following Ref. [29]. Equation (21) is valid for any distribution of the scattering spheres. In addition, the spheres can have different radii.

C. Approximations

1. Approximation for tenuous media

From Eq. (21), the total wave reaching a receiver can be written as

$$p(\vec{r},\omega) = p^0(\vec{r},\omega) + \sum_{i=1}^{N} p_s(\vec{r}_i;\vec{r},\omega), \tag{22}$$

where $p^0(\vec{r},\omega)$ is the direct wave arriving at the receiver and the summation term represents the scattered waves from scatterers.

When $k|\vec{r}-\vec{r}_i| \gg 1$, valid for tenuous media, the above derivation can be simplified. The scattered wave from each target, say the ith target, can be generically written as

$$p_s(\vec{r}_i;\vec{r},\omega) = p^0(\vec{r}_i,\omega)F_i(\vec{r}_i,\vec{r};\vec{k}_{in})\frac{e^{ik|\vec{r}-\vec{r}_i|}}{|\vec{r}-\vec{r}_i|}, \tag{23}$$

where F_i is the effective scattering function of the ith target. Using

$$h_l^{(1)}(x) \to \frac{1}{kx}\exp[ikx - i(l+1)\pi/2], \quad \text{as} \quad x\to\infty,$$

we have from Eq. (10)

$$F_i(\vec{r}_i,\vec{r};\vec{k}_{in}) = \sum_{l=0}^{\infty}\sum_{m=-l}^{m=l} C_{lm}^i \frac{1}{kp^0(\vec{r}_i,\omega)} \times Y_l^m([\theta,\phi]_i)e^{-i(l+1)\pi/2}. \tag{24}$$

Equation (23) is also called the far-field approximation. Without multiple scattering among targets, F_i will be equal

to the bare scattering function of the single target $f_i(\vec{r}_i,\vec{r};\vec{k}_{in})$ that, obtained when other targets are absent, is readily derived as

$$f_i(\vec{r}_i,\vec{r};\vec{k}_{in})=\sum_{l=0}^{\infty}\sum_{m=-l}^{m=l}(-\Gamma_l)S_{lm}^i\frac{1}{kp^0(\vec{r}_i,\omega)}Y_l^m([\theta,\phi]_i). \tag{25}$$

Here we used the fact that when there are no other scatterers, the incident wave on any scatterer will be just be that from the source. Thus we have from Eq. (14)

$$D_{lm}^i=S_{lm}^i \tag{26}$$

and then Eq. (20) yields

$$D_{lm}^i=-\Gamma_l S_{lm}^i. \tag{27}$$

Note here that $f_i(\vec{r}_i,\vec{r};\vec{k}_{in})$ is interpreted as the scattering function of the ith target in the scattering direction $\vec{r}-\vec{r}_i$ when the incidence is along the direction of $\vec{k}_{in}$, whereas $F_i(\vec{r}_i,\vec{r};\vec{k}_{in})$ is the effective scattering function incorporating multiple scattering from other targets.

On the other hand, the scattered wave from the ith target is a linear response to the total incident wave incident on the target, which as a result of multiple scattering includes the direct incident wave and the scattered wave from other targets, and can be thus written alternatively as

$$p_s(\vec{r}_i;\vec{r},\omega)=Q(\vec{r}_i;\vec{r})\frac{e^{ik|\vec{r}-\vec{r}_i|}}{|\vec{r}-\vec{r}_i|} \tag{28}$$

with

$$Q(\vec{r}_i;\vec{r})=f_i(\vec{r}_i,\vec{r};\vec{k}_{in})p^0(\vec{r}_i,\omega)+\sum_{j=1,j\neq i}^{N}p^0(\vec{r}_j,\omega)f_i(\vec{r}_i,\vec{r};\hat{r}_i-\hat{r}_j)\times F_j(\vec{r}_j,\vec{r}_i;\vec{k}_{in})\frac{e^{ik|\vec{r}_i-\vec{r}_j|}}{|\vec{r}_i-\vec{r}_j|}. \tag{29}$$

Equating Eqs. (23) and (28), we get

$$F_i(\vec{r}_i,\vec{r};\vec{k}_{in})=f_i(\vec{r}_i,\vec{r};\vec{k}_{in})+\sum_{j=1,j\neq i}^{N}\frac{p^0(\vec{r}_j,\omega)}{p^0(\vec{r}_i,\omega)}f_i(\vec{r}_i,\vec{r};\hat{r}_i-\hat{r}_j)\times F_j(\vec{r}_j,\vec{r}_i;\vec{k}_{in})\frac{e^{ik|\vec{r}_i-\vec{r}_j|}}{|\vec{r}_i-\vec{r}_j|}. \tag{30}$$

Setting $\vec{r}$ at the targets except the ith, we obtain $N-1$ equations

$$F_i(\vec{r}_i,\vec{r}_l;\vec{k}_{in})=f_i(\vec{r}_i,\vec{r}_l;\vec{k}_{in})+\sum_{j=1,j\neq i}^{N}\frac{p^0(\vec{r}_j,\omega)}{p^0(\vec{r}_i,\omega)}\times f_i(\vec{r}_i,\vec{r}_l;\hat{r}_i-\hat{r}_j)F_j(\vec{r}_j,\vec{r}_i;\vec{k}_{in})\frac{e^{ik|\vec{r}_i-\vec{r}_j|}}{|\vec{r}_i-\vec{r}_j|};\quad (l=1,2,\ldots,N,\ \text{except}\ l=i.) \tag{31}$$

Now in each of the $N-1$ equations, we allow i to vary from 1 to N. Then we have other N equations. In total we would have $(N-1)\times N$ equations for $N(N-1)$ unknown coefficients $F_j(\vec{r}_j,\vec{r}_i;\vec{k}_{in})$:

$$F_i(\vec{r}_i,\vec{r}_l;\vec{k}_{in})=f_i(\vec{r}_i,\vec{r}_l;\vec{k}_{in})+\sum_{j=1,j\neq i}^{N}\frac{p^0(\vec{r}_j,\omega)}{p^0(\vec{r}_i,\omega)}\times f_i(\vec{r}_i,\vec{r}_l;\hat{r}_i-\hat{r}_j)F_j(\vec{r}_j,\vec{r}_i;\vec{k}_{in})\frac{e^{ik|\vec{r}_i-\vec{r}_j|}}{|\vec{r}_i-\vec{r}_j|};\quad (i,l=1,2,\ldots,N;i\neq j.) \tag{32}$$

The scattering function $F_i(\vec{r}_i,\vec{r}_l;\vec{k}_{in})$ can be solved from the self-consistent equation (32). Then the total wave at any spatial point is given by

$$p(\vec{r},\omega)=p^0(\vec{r},\omega)+\sum_{i=1}^{N}p^0(\vec{r}_i,\omega)F_i(\vec{r}_i,\vec{r};\vec{k}_{in})\frac{e^{ik|\vec{r}-\vec{r}_i|}}{|\vec{r}-\vec{r}_i|}. \tag{33}$$

2. Low frequency limit

When we consider the most interesting low frequency acoustic scattering in bubble water, the problem can be further simplified. In this case, the tenuous approximation can be relaxed. It is found for frequencies satisfying $(\omega/c)a<0.4$, only $l=0$ mode in the bubble scattering is important [30]. More explicitly, for $(\omega/c)a<0.4$ below roughly about 0.4, the acoustic scattering by an air bubble in water can be well mimicked by the scattering by a radially vibrating sphere. The error in such approximation is less than a few percent. In this situation, the bubble physically behaves like a resonating sphere. The pulsating mode dominates the scattering. In this case, the scattered wave from the ith bubble without other bubbles can be written as

$$p_s(\vec{r}_i,\vec{r})=p^0(\vec{r}_i,\omega)f_i\frac{e^{ik|\vec{r}-\vec{r}_i|}}{|\vec{r}-\vec{r}_i|}, \tag{34}$$

where f_i is the isotropic scattering function of the bubble without other bubbles' presence and can be computed as [21]

$$f_i=\frac{a_i}{\omega_{0,i}^2/\omega^2-1-ika_i}, \tag{35}$$

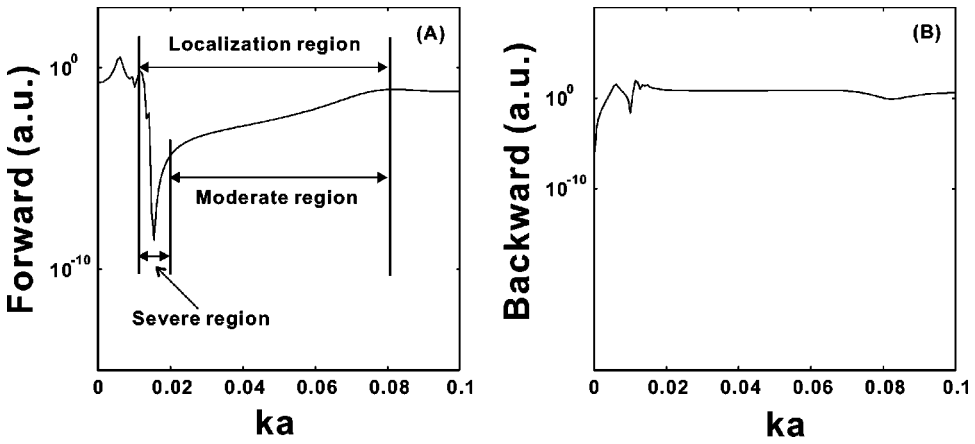

FIG. 1. Transmission (a) and backscattering (b) as a function of ka.

where $\omega_{0,i}$ is the natural frequency of the ith bubble. Under the normal conditions, i.e., at the pressure of one atmosphere and the room temperature, the nature frequency is determined as

$$(\omega_{0,i}/c)a_i \approx 0.0136. \tag{36}$$

When other bubbles are present, the scattered wave is written as

$$p_s(\vec{r}_i,\vec{r}) = p^0(\vec{r}_i,\omega)F_i \frac{e^{ik|\vec{r}-\vec{r}_i|}}{|\vec{r}-\vec{r}_i|}. \tag{37}$$

In this case, Eq. (32) can be simplified into

$$F_i = f_i + \sum_{j=1,j\neq i}^{N} \frac{p^0(\vec{r}_j,\omega)}{p^0(\vec{r}_i,\omega)} f_i F_j \frac{e^{ik|\vec{r}_i-\vec{r}_j|}}{|\vec{r}_i-\vec{r}_j|};$$
$$(i,l=1,2,\ldots,N; i\neq j). \tag{38}$$

Once F_i is obtained, the pressure field at any spatial point can be derived as

$$p(\vec{r},\omega) = p^0(\vec{r},\omega) + \sum_{i=1}^{N} p^0(\vec{r}_i,\omega)F_i \frac{e^{ik|\vec{r}-\vec{r}_i|}}{|\vec{r}-\vec{r}_i|}. \tag{39}$$

III. NUMERICAL MODEL AND RESULTS

A. The model

In the following, we restrict our attention to the scattering at low frequencies, i.e., $ka<0.4$. The numerical model is set up as follows. Consider a point acoustic source in bubbly water. The source is assumed to be at the origin. There are N spherical air-filled bubbles of the same radius and these bubbles are randomly distributed within a spatial domain, which is taken as the spherical shape. We require that no two bubbles occupy the same spot. In other words, the point source is placed at the center of a spherical bubble cloud; such a model actually describes the acoustic noise naturally generated inside the bubble clouds in the upper ocean processes. The reason why the source is placed inside rather than outside the bubble cloud is that only in this way the problem of whether the transmitted waves can indeed be trapped inside the medium can be investigated without ambiguity and we will be able to isolate the localization effect from boundary effects. The radius of the bubbles is a. The volume fraction, the fraction of volume occupied by the bubbles per unit volume is β. Therefore the numerical density of the bubbles is $n=3\beta/4\pi a^3$ and the radius of the bubble cloud is $R/a=(N/\beta)^{1/3}$. In the following, we study the total acoustic field given by Eqs. (9) and (21).

B. The results

For reference, first we repeat the case of a unit point source transmitting a continuous monochromatic wave of angular frequency ω. A set of numerical experiments has been carried out for various bubble sizes, numbers and concentrations. The locations of the bubbles are randomly generated within the prescribed sphere by the computer, to simulate the random configurations of the bubble cloud. We found that all features are qualitatively the same for any random configurations. As an example, Fig. 1 shows typical results for wave transmission and backscattering as a function of frequency in terms of ka. Hereafter, ''a.u.'' stands for ''arbitrary unit.'' In this simulation, we take $\beta=10^{-3}$, and $N=200$. The radius of the bubble can be used as the length unit in the simulation. Here we see that in a range of frequencies the wave transmission is greatly inhibited. This is the range that suggests the wave localization [21]. A further numerical computation discovers such a range appears as long as β is greater than about 10^{-5} [31]. For the backscattering situation the result shows that the backscattering signal persists for all the frequencies. In this particular case, the range of inhibition is $ka=0.014$–0.08. While the waves are moderately localized between $ka=0.02$ and 0.08, the most severe inhibition occurs between 0.014 and 0.02. In general, the localization range is widened as β increases.

Now consider the pulse propagation. A number of pulse shapes are considered and yield the same qualitative features. In the following, we present the results for the broad band pulse given by Eq. (5). The following parameters are used: $\alpha=5\times10^{-7}$ and $\beta=10^{-3}$. The number of bubbles varies from 100 to 400. Greater number of bubbles is possible, only to take more computing time. In the simulation, all lengths are scaled by the radius of bubbles. Figure 2 shows the time series of the transmitted, forwardly and backwardly received

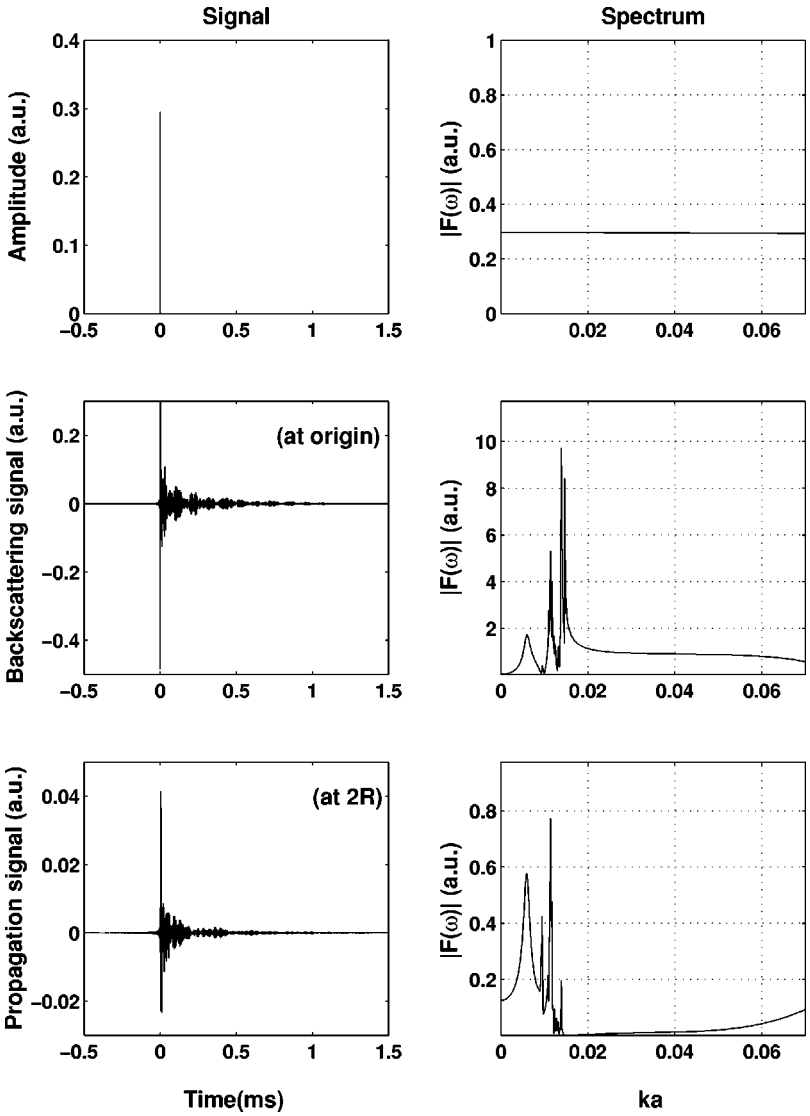

FIG. 2. Time series of the signals. Left column from bottom to top: the transmitted signal, the signal received at the transmitting site (backscattering), and the signal received at the point $2R$. Right: the corresponding power spectra for the signals shown in the left column.

signals and their power spectra, respectively. The forward receiver is located at $2R$ from the cloud. From the figure, it is clear that as a signal is transmitted, the backscattered signal is significantly greater than that received outside the bubble cloud, an indication of enhanced backscattering in line with the previous discussion. A very short pulse generates a relatively long response in both the forward and backward signals. For the backscattering the greatest portion of the signal is within the range of frequencies in which the transmission is most severely inhibited, referring to Fig. 1. In contrast, in the forward direction, the transmitted waves do not have much this portion of frequencies. The most significant forward signal is located around the resonance frequency of the single bubble, referring to Eq. (36); this is because at these frequencies the scattering is very strong. These results hint that when a pulse is transmitted, the waves of frequencies within the localized regime will be strongly backscattered, while those with frequencies outside this regime can be transmitted outward. Due to the finite size of the cloud, waves in the moderately inhibited region can still leak out. This is why we only observe a narrow dip rather than the whole localization range in the forward signal; when the sample size is increased, more waves within the localization regime will be trapped and the dip will be widened.

We now study the residual signals, i.e., the signals that remain inside the bubble cloud, by considering the time series of the signals after the pulses are transmitted for a period of time; in this way we can investigate what portions of the signals remain inside the bubble cloud. It is clear that without the bubbles, the transmitted waves will all leave the system and there will be no residual signals in the system. In the presence of bubbles, due to multiple scattering some waves will reverberate inside and around the system. Figure 3 shows the time series of the signals for one random distribution of bubbles at $0.1R$ and $2R$, corresponding the cases when the receiver is located inside and outside the bubble cloud, respectively. The time series is plotted 1 ms after a pulse is fired, a period considerably long after the pulse is generated. From the left diagram, we find that there indeed exist the residual signals. On the right side of the figure, the Fourier analysis of the signals shows that the main portions of the signals in the frequency spectra are well within the most localized regime indicated by Fig. 1. In other words, these signals reflect the waves that are most localized inside

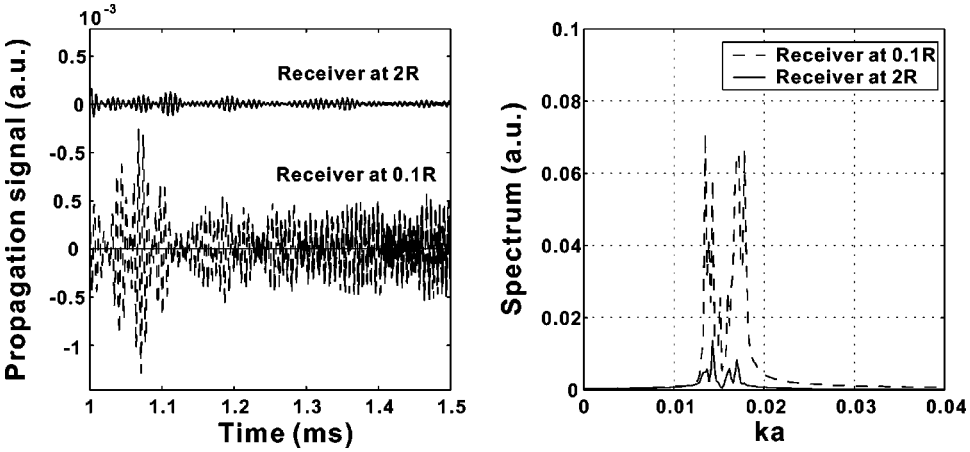

FIG. 3. The residual time series of signal received at 0.1R (inside the cloud) and 2R (outside the cloud).

the bubble cloud. As the localization length is a function of frequency, the more localized is the wave, the shorter is the localization length and the stronger is the residual signal. In the figure, the residual signal is contributed mostly from the waves between $ka=0.014$ and $ka=0.02$. The waves at other localization frequencies have longer localization lengths. In order to trap the waves with long localization length, the sample should be sufficiently large. Figure 3 also shows that the signal received at $2R$ (i.e., outside the cloud) is significantly smaller than that being received at $0.1R$. This is expected, as the further away from the transmitting site, the less energy will be received for the localized waves.

To further explore the signals observed in Fig. 3, we consider the backscattering signal, i.e., the signal received at the transmitting site, for different sample sizes. The typical numerical results are presented in Fig. 4. The time series is taken at 1 ms after a pulse is transmitted. As shown by these results, the increase in the size of the bubble cloud leads to an increase in the residual signal. This indicates that as the sizes increases, the localization effect becomes stronger. The left portion of Fig. 4 shows that the greater is the sample size, the wider is the power spectrum of the residual signal. We expect that as the sample size increases, the frequency spectrum will become wider and wider and eventually all waves in the localization region will be trapped inside the medium.

We can also study the phase behavior of the acoustic fields. In terms of wave field p, the energy flow in the system is calculated from $\vec{J}(\vec{r})\sim \mathrm{Re}[p(\vec{r})i\nabla p(\vec{r})]$. Writing $p=|p|e^{i\theta}$, the flow becomes $\vec{J}\sim|p|^2\nabla\theta$. Clearly, when θ is a constant and $|p|$ is nonzero, the energy flow stops, i.e., $\vec{J}=0$, and the wave is then localized or frozen in the space. Therefore an investigation of the phase behavior of the acoustic field will provide useful information about the localization effect. Consider the signal received at an arbitrary point $\vec{r}$, described by $F(\vec{r},t)$ say. Its Fourier component is determined by

$$f(\vec{r},\omega)=\int dt\, e^{i\omega t}F(\vec{r},t). \tag{40}$$

We rewrite

$$f(\vec{r},\omega)=|f(\vec{r},\omega)|\exp[i\theta(\vec{r},\omega)]. \tag{41}$$

For the phase field, we define a unit phase vector

$$\vec{u}(\vec{r},\omega)=\cos\theta(\vec{r},\omega)\vec{e}_x+\sin\theta(\vec{r},\omega)\vec{e}_y. \tag{42}$$

We will then plot the phase vector versus various frequencies at different spatial points for different random realizations of the bubble cloud. Here we consider the time series of the signals from 1 ms after the pulse is transmitted. A typical set of results is shown in Fig. 5. Here we show the phase diagrams for three frequency ranges at two spatial points inside

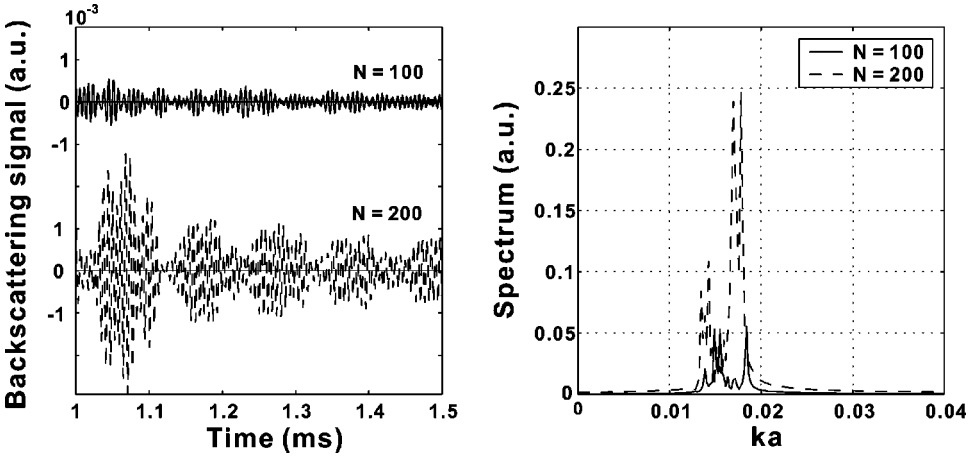

FIG. 4. The residual time series of the backscattered signal for two bubble numbers.

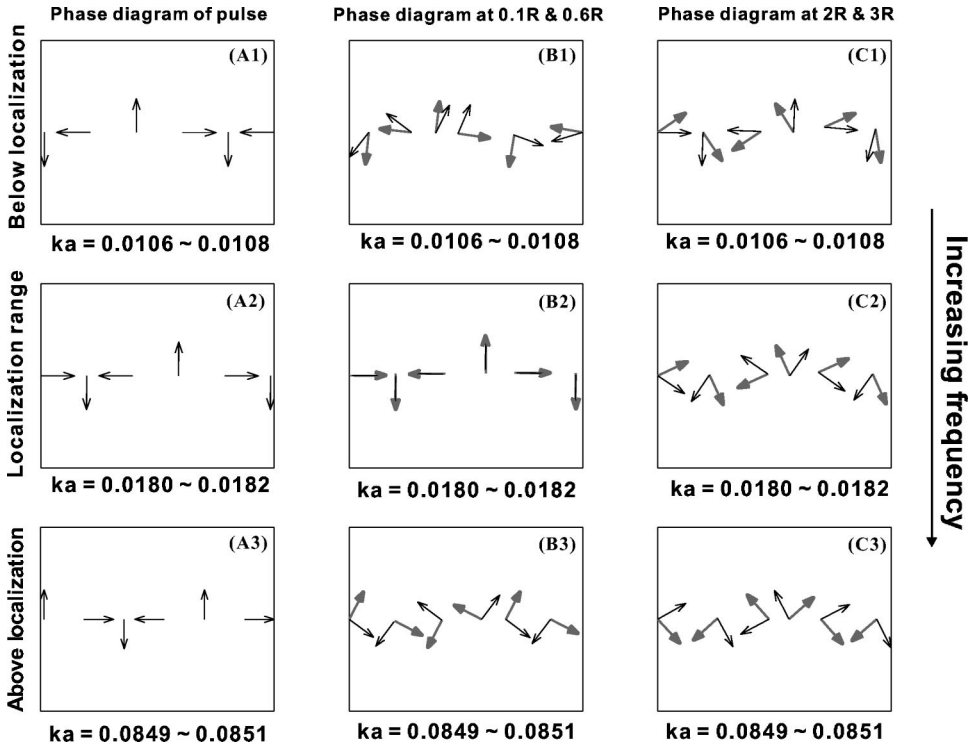

FIG. 5. The phase diagrams for signal received at various spatial points and for various frequency ranges.

the bubble cloud at $0.1R$ and $0.6R$, and two points located outside the cloud at $2R$ and $3R$. To save the computing time yet without losing the essence of the problem, we only plot the results for $N=200$. The three ranges of frequencies are located below, within, and above the localization regime, respectively. For example, the range of ka from $ka=0.0106$ to 0.0108 refers to that below, that from 0.0180 to 0.0182 to within, and that from 0.0849 to 0.0851 to above the localization regime.

On the left are the phase vectors for the transmitted pulse. Due to the nature of the pulse, the phase vectors point to various directions for different frequencies. The phase vectors for the acoustic waves inside the cloud are presented in the middle column. On the figure the full-headed arrows in lighter gray refer to the phase vectors at $0.1R$ while the normal arrows refer to the phase vectors at $0.6R$. Here the results demonstrate that for both below and above the localization range (B1 and B3), the phase vectors point to different directions at different locations and are not in any coherence with the phase vectors of the transmitting source. Within the localization regime, however, the phase vectors for the two locations inside the cloud coincide with each other, as shown in (B2). As a matter of fact, they are in the same phase as the acoustic source. Physically, this means that the field oscillates in the same phase of the source. We have performed more simulations and conclude that once within the localization range the acoustic field at all spatial points inside the bubble cloud tends to oscillate completely in phase with the source. Such a coherence behavior prohibits waves from propagation and effectively traps waves; no work can be done when the medium moves in the same phase as the source. However, we must stress that as the sample is inevitably finite, the waves within the moderate localization range can still leak out from the system. In this case, the in-phase feature such as that shown by B2 becomes less evident. For example, although the frequencies ranging from $ka=0.07$ to 0.08 are within the localization regime as shown by Fig. 1, the localization effect at these frequencies is too moderate to exhibit the in-phase behavior. But, when the sample size is increased, the coherence in the phase vectors is expected to appear.

The ordering in the phase vectors guarantees that the zero time lag is the prominent peak position of the correlation between the time series at any two spatial points. To be explicit, consider two arbitrary real time series $f(t)$ and $g(t)$. Their Fourier transforms are $f(\omega)$ and $g(\omega)$. The time correction of the two series is

$$F(\tau)=\int dt\, f(t)g(t+\tau). \tag{43}$$

This can be evaluated as

$$F(\tau)=\int d\omega\, f(\omega)g^{\star}(\omega)e^{-i\omega\tau}. \tag{44}$$

When $f(\omega)$ and $g(\omega)$ are in phase, the fact that $F(\tau)$ is a real function leads to $dF(\tau)/d\tau|_{\tau=0}=0$. The second time derivative at zero time lag is

$$\left.\frac{d^2F(\tau)}{d\tau^2}\right|_{\tau=0}=-\int d\omega\,\omega^2 f(\omega)g^{\star}(\omega). \tag{45}$$

As $f(\omega)$ and $g(\omega)$ are in phase, we have

$$\left.\frac{d^2F(\tau)}{d\tau^2}\right|_{\tau=0}<0. \tag{46}$$

Therefore $F(\tau)$ at zero time lag $\tau=0$ is a maximum. In experiments, this feature may serve as an indication for the wave localization or trapping.

For points located outside the cloud, there is no phase ordering in the received time series for all frequency components. In fact, once waves leak out from the bubble cloud, they start to propagate toward infinity. In this situation, the oscillation phase of acoustic waves will be position dependent. These are clearly illustrated by the right column of Fig. 5. Here the full-headed and normal arrows refer to the phase vectors at $2R$ and $3R$, respectively. The out-of-phase property indicates that there is energy flow outside the bubble cloud. This energy flow must be a result of wave leaking from the system, due to the finite size of the system. That there is energy flow even for frequencies within the most localized regime (C2) implies that for a finite system the in-phase behavior at these frequencies shown by B2 will degrade as the time elapses and all waves will leak out eventually.

Finally, we emphasize that all the above features associated with the phase vectors hold for any random realization of the bubble clouds. We also note that in the simulation the acoustic absorption caused by the viscosity and thermal exchange is neglected. This is a valid assumption when the bubbles are not too small [31]. The absorption will degrade the in-phase behavior.

IV. SUMMARY

We studied the localization behavior of acoustic pulses in random bubble water using a self-consistent approach. The results show that after a signal is transmitted, waves within the localized regime contribute to the residual acoustic reverberation in the system for any random configuration of bubble clouds in water. These waves are actually trapped or localized inside the system. The degree of wave trapping effect is sensitive to the frequency, the sample sizes, and the bubble concentrations. It is also found that once localized, the field tends to oscillate in phase at any spatial points. In other words, the localized waves behave as a standing wave inside the random medium. This is supported by a simple theoretical argument. The coherence phenomenon is a unique feature associated with the wave localization and may be used to distinguish the localization effect from the residual absorption effect.

ACKNOWLEDGMENT

The work received support from National Science Council.

[1] L. L. Foldy, Phys. Rev. **67**, 107 (1945).
[2] M. Lax, Rev. Mod. Phys. **23**, 287 (1951).
[3] P. C. Waterman and R. Truell, J. Math. Phys. **2**, 512 (1961).
[4] V. Twersky, J. Math. Phys. **3**, 700 (1962).
[5] U. Frisch, in *Probabilities Methods in Applied Mathematics*, edited by A. T. Barucha-Reid (Academic, New York, 1968).
[6] P. W. Anderson, Phys. Rev. **109**, 1492 (1958).
[7] P. A. Lee and T. V. Ramakrishnan, Rev. Mod. Phys. **57**, 287 (1985).
[8] T. R. Kirkpatrick, Phys. Rev. B **31**, 5746 (1985).
[9] C. A. Condat, J. Acoust. Soc. Am. **83**, 441 (1988).
[10] D. Sornette and B. Souillard, Europhys. Lett. **7**, 269 (1988).
[11] P. Sheng and M. Y. Zhou, Science **253**, 539 (1991).
[12] A. Z. Genack and N. Garcia, Phys. Rev. Lett. **66**, 2064 (1991).
[13] R. Dalichaouch, J. P. Armstrong, S. Schultz, P. M. Platzman, and S. L. McCall, Nature (London) **354**, 53 (1991).
[14] A. Lagendijk and B. A. van Tiggelen, Phys. Rep. **270**, 143 (1996).
[15] S. John, Phys. Today **44** (5), 32 (1991).
[16] P. Sheng, *Introduction to Wave Scattering, Localization and Mesoscopic Phenomena* (Academic Press, New York, 1995).
[17] Y. Kuga and A. Ishimaru, J. Opt. Soc. Am. A **1**, 831 (1984); M. van Albada and A. Lagendijk, Phys. Rev. Lett. **55**, 2692 (1985); P. E. Wolf and G. Maret, *ibid.* **55**, 2696 (1985); A. Tourin *et al.*, *ibid.* **79**, 3637 (1997).
[18] M. Torres, J. P. Adrados, and F. R. Montero de Espinosa, Nature (London) **398**, 114 (1999).
[19] D. S. Wiersma, P. Bartolini, A. Lagendijk, and R. Roghini, Nature (London) **390**, 671 (1997).
[20] C. H. Hodges and J. Woodhouse, J. Acoust. Soc. Am. **74**, 894 (1983).
[21] Z. Ye and A. Alvarez, Phys. Rev. Lett. **80**, 3503 (1998); Z. Ye, H. R. Hsu, E. Hoskinson, and A. Alvarez, Chin. J. Phys. (Taipei) **37**, 343 (1999).
[22] A. Ishimaru, *Wave Propagation and Scattering in Random Media* (Academic Press, New York, 1978).
[23] Z. Ye, J. Acoust. Soc. Am. **102**, 1239 (1997); Z. Ye and C. Feuillade, *ibid.* **102**, 798 (1997).
[24] F. Scheffold, R. Lenke, R. Tweer, and G. Maret, Nature (London) **398**, 206 (1999); D. Wiersma, *et al.*, *ibid.* **398**, 207 (1999); A. A. Chabanov, M. Stoytchev, and A. Z. Genack, *ibid.* **404**, 850 (2000).
[25] T. G. Leighton, *The Acoustic Bubble* (Academic Press, New York, 1994).
[26] Z. Ye and L. Ding, J. Acoust. Soc. Am. **98**, 1629 (1995).
[27] F. S. Henyey, J. Acoust. Soc. Am. **105**, 2149 (1999).
[28] I. S Gradshteyn, I. M. Ryzhik, and A. Jeffrey, *Table of Integrals, Series, and Products*, 5th ed. (Academic Press, New York, 1994).
[29] J. J. Faran, J. Acoust. Soc. Am. **23**, 495 (1951).
[30] Z. Ye, J. Acoust. Soc. Am. **101**, 1945 (1997).
[31] A. Alvarez and Z. Ye, Phys. Lett. A **252**, 53 (1999).